Progress In Electromagnetics Research B, Vol. 32, 57–73, 2011

BOWTIE NANOANTENNAS WITH POLYNOMIAL SIDES IN THE EXCITATION AND EMISSION REGIMES

K. Q. Costa* **and V. A. Dmitriev**

Department of Electrical Engineering, Federal University of Para, Augusto Correa Str. 1, Belem Para, Brazil

Abstract—In this work, we analyze modified bowtie nanoantennas with polynomial sides in the excitation and emission regimes. In the excitation regime, the antennas are illuminated by an incident plane wave, and in the emission regime, the excitation is fulfilled by infinitesimal electric dipole positioned in the gap of the nanoantennas. Several antennas with different sizes and polynomial order were numerically analyzed by method of moments. The results show that these novel antennas possess a controllable resonance by the polynomial order and good characteristics of near field enhancement and confinement for applications in enhancement of spontaneous emission of a single molecule.

1. INTRODUCTION

Nanoantennas are metal nanostructures used to enhance, confine, receive, and transmit optical fields [1]. Potential applications of nanoantennas are ultra-high-density optical data storage devices [2], super-resolution microscopy [3], integrated nano-optical devices [4], optical communication between functional elements of nanometer size [5], chemical enhancement for surface-enhanced Raman scattering [6], and biology [7]. Increasing investigations in this field in the last years is due to the promising applications, the development of modern techniques of micro and nanofabrication tools such as focused ion beam milling (FIB), and increasing the capabilities of numerical techniques of analysis.

One important application of nanoantennas is to enhance the spontaneous emission of a single molecule. In this process, a molecule

Received 28 March 2011, Accepted 30 June 2011, Scheduled 6 July 2011

* Corresponding author: Karlo Queiroz Da Costa (karlo@ufpa.br).

positioned near a given antenna is excited by the high local field of the antenna. The analysis of this process can be divided in two regimes: excitation and emission ones. In the first regime, an incident plane wave illuminates the antenna and the near field enhancement is the phenomenon to be investigated. In the second regime, the emitter localized near the antenna is modeled by an infinitesimal electric dipole, and the radiation efficiency is the object of interest. The whole emission performance of the emitter depends on these two processes.

Some conventional nanoantennas that have good characteristics for the enhancement of spontaneous emission of a single molecule are linear and bowtie dipoles. Several works have been analyzed linear nanodipoles with different geometric parameters in the excitation regime [8, 9] and emission regime [10–13]. The characteristics of bowtie nanoantennas with different length, bow angles, radius of curvature of the apex, and gap distance in the excitation regime are presented in [9, 14, 15], and in the emission regime are discussed in [16, 17].

In this paper, we investigate Au modified bowtie nanoantennas in the excitation and emission regimes. The proposed antennas possess polynomial sides instead of linear ones of the conventional triangular antenna. We study numerically several modified antennas with different sizes and polynomial order by method of moments (MoM). The analyzed parameters are as follows: spectral response, near field enhancement and confinement, radiation efficiency and directivity.

2. THEORY

2.1. Geometry of the Modified Bowtie Nanoantennas

The geometries of the modified bowtie nanoantennas are shown in Figure 1. In this figure, four antennas made of Au with different values of the parameter $\alpha = (1, 2, 3, 4)$ are presented, where α is the polynomial order of the sides variation. The polynomial function used to model the curvature of the sides is $x = (y/k_1)^{\alpha}$, where $k_1 = L/2h^{1/\alpha}$, $h = 0.5L(3)^{0.5}$, L is the side length of the conventional bowtie equilateral triangle. The conventional bowtie antenna corresponds to the case $\alpha = 1$ where the side variation is linear. These antennas are placed in the origin of the coordinate system with the axis of the antenna oriented along the x axis. The distance between the arms of the bowtie dipoles is d, and the thickness in z-direction which is not shown, is w. With these parameters, the total antenna's length is $d + 2h$. For higher values of α, the tips of the antenna are more acute. The surrounding medium where the antennas are placed is the air. It

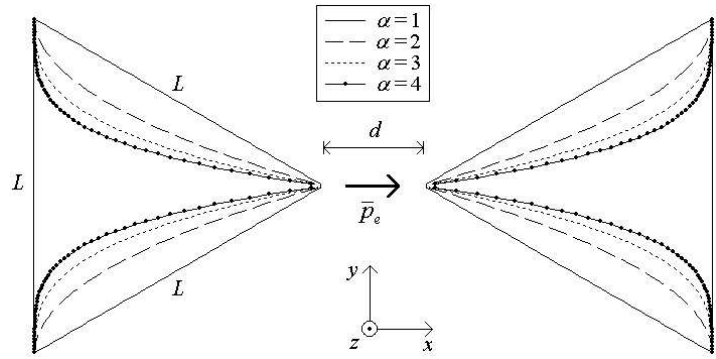

Figure 1. Geometries of the bowtie nanoantennas with polynomial sides. The form of the sides varies as the function $x = (y/k_1)^{\alpha}$, where $k_1 = L/2h^{1/\alpha}$, $h = 0.5L(3)^{0.5}$. The conventional case is $\alpha = 1$.

is known that the principal effect of substrate on a given antenna is to increase its resonant wavelength [9]. Therefore, to simplify the analysis and to investigate only the influence of geometry on the antenna characteristics, we consider the structure without substrate.

2.2. Numerical Model

There are several numerical methods to analyze nanoantennas. Examples of such methods are the Green's tensor method with volume integral equation [18–21], boundary integral method [22], finite-difference time domain [23], discrete-dipole approximation [24], and finite integration technique [25].

The nanoantennas shown in Figure 1 were numerically analyzed by a MoM code based on the model proposed in [18]. In this model, the equivalent polarization current inside the total volume v of the antennas $\bar{J}_{eq} = j\omega[\epsilon(\bar{r}) - \epsilon_0]\bar{E}(\bar{r}) = \tau(\bar{r})\bar{E}(\bar{r})$ is determined by solving the tensor integral equation for the electric field

$$\left[1 + \frac{\tau(\bar{r})}{3j\omega\epsilon_0}\right]\bar{E}(\bar{r}) - PV\int_v \tau(\bar{r}')\bar{E}(\bar{r}')\cdot\bar{G}(\bar{r},\bar{r}')dv' = \bar{E}^i(\bar{r}) \quad (1)$$

In (1), PV means the principal value of the integral where the evaluation is inside the volume v excluding the singularities of the free space vector Green's function $\bar{G}$. The variables and parameters in (1) are as follows: $\bar{E}^i$ and $\bar{E}$ are the incident and total electric field inside the volume v, respectively, ω the angular frequency, $k_0 = \omega(\mu_0\epsilon_0)^{1/2} = 2c\pi/\lambda$ the wave number in the air, λ is the wavelength, c is the speed of the light in free space, μ_0 the free space permeability, ϵ_0 the free

space permittivity. The complex permittivity of the Au antennas is $\epsilon = \epsilon_0 \epsilon_r$, where ϵ_r is defined

$$\epsilon_r = \epsilon_\infty - \frac{\omega_{p1}^2}{\omega^2 - j\Gamma\omega} + \frac{\omega_{p2}^2}{\omega_0^2 - \omega^2 + j\gamma\omega} \tag{2}$$

and the parameters of this equation are: $\epsilon_\infty = 7$, $\omega_{p1} = 13.8 \times 10^{15}\,\mathrm{s}^{-1}$, $\Gamma = 1.075 \times 10^{14}\,\mathrm{s}^{-1}$, $\omega_0 = 2c\pi/\lambda_0$, $\lambda_0 = 450\,\mathrm{nm}$, $\omega_{p2} = 45 \times 10^{14}\,\mathrm{s}^{-1}$, and $\gamma = 9 \times 10^{14}\,\mathrm{s}^{-1}$ [1]. This model is a good approximation in the range of wavelengths from 500 nm to 1800 nm. In this frequency range we fulfill our analysis.

The excitation of the antennas is represented by $\bar{E}^i$. Two kinds of sources are considered in this model: an Ex-polarized, z-directed plane wave, and an infinitesimal electric dipole with moment $\bar{p}_e$ positioned in middle of the gap's antenna and polarized in the x axis (Figure 1). The first numerical experiment is called the excitation regime and the second the emission regime.

To solve these scattering problems by MoM, the volume of a given antenna is divided in N small cubic subvolumes Δv, where the total electric field is approximately constant. With this approximation, the integral equation is transformed into a linear system with $N_t = 3N$ equations because there are three electric field components in each subvolume.

The curved sides of the antennas are approximated by staircase due the cubic subvolume discretization. The corners of the antenna's geometries in the numerical simulations possess finite radius of curvatures because in these points there are a small number of cubic subvolumes. Thus, the radius of curvature depends on the size of the cubic subvolumes Δv. It is important to comment here that we do not consider non local effects that can occur in the sharp corners. This effect can be taking into account by using the non local dielectric function model presented in [15].

The validation of this model was done by comparing the simulation results for the case of a gold sphere with the analytical Mie solution [26]. We also did a comparison with a numerical example presented in [9]. The results of the normalized field enhancement $(|\bar{E}|/|\bar{E}_{\max}|)^2$ in the middle of a conventional bowtie nanodipole is shown in Figure 2. We observe a good concordance near the principal resonance $\lambda_{res} = 715\,\mathrm{nm}$. We believe that the differences in these two results are due to differences in the numeric models used to solve the scattering problem and also due to different models of permittivity.

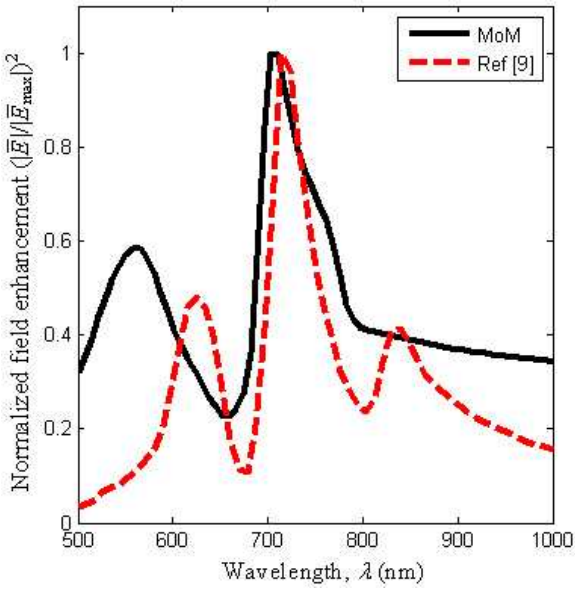

Figure 2. Spectral response of the normalized near field enhancement $(|\bar{E}|/|\bar{E}_{\max}|)^2$ in the middle of a bowtie nanodipole with $h = 40\,\text{nm}$, $w = 40\,\text{nm}$, $d = 30\,\text{nm}$, and *bowangle* $= 90°$. The continuous curve was obtained here and the traced curve was obtained in [9].

2.3. Definition of the Analyzed Parameters

The solution of the equivalent linear system produces the total electric field $\bar{E}$ inside the volume v of the antenna. With this result, the near and far field characteristic parameters of the antennas are calculated. In the excitation regime, we calculated the near electric field and scattering cross section respectively by

$$\bar{E}^t(\bar{r}) = \bar{E}^i(\bar{r}) + \int_v \tau(\bar{r}')\bar{E}(\bar{r}') \cdot \bar{G}(\bar{r}, \bar{r}')dv' \tag{3}$$

$$SCS(\theta, \phi) = 8\pi\eta U(\theta, \phi)/|\bar{E}^i|^2 \tag{4}$$

where η is the free space impedance and $U(\theta, \phi)$ is the radiation intensity of the scattered far field in a given direction θ and ϕ.

Other characteristics analyzed in this regime are the field enhancement and spatial confinement. The first one is defined by $(|\bar{E}^t|/|\bar{E}_0|)^2$, where $|\bar{E}^t|$ is the amplitude of the total field near the antenna and $\bar{E}_0$ is the amplitude of the incident plane wave. The second characteristic is a spatial distance between 3 dB points where $(|\bar{E}^t|/|\bar{E}_0|)^2 = 0.5$. This parameter is a spatial bandwidth (in

nanometers) around the maximum field enhancement. In case of the nanoantennas, this maximum value is in the middle of the antenna's gap. In the present analysis, we calculated the spatial confinement in the axis y and z (Figure 1) and we represent them by σ_y and σ_z, respectively.

In the emission regime, we evaluated the directivity D and radiation efficiency e by [27]

$$D(\theta,\phi) = 4\pi U(\theta,\phi)/P_{rad} \quad (5)$$

$$e(\%) = 100 \times P_{rad}/(P_{loss}+P_{rad}) \quad (6)$$

where $P_{rad} = \int_0^{2\pi}\int_0^{\pi} U d\theta d\phi$ and $P_{loss} = \mathrm{Re}(-0.5j\omega\epsilon^* \int_v |\bar{E}|^2 dv)$ are the radiated and dissipated power of the antennas. In (6), the characteristic U is the total radiation intensity due to the scattered field by the antenna and the radiated field by the infinitesimal electric dipole.

3. NUMERICAL RESULTS

Based on the theory presented in the previous section, we simulated several nanoantennas with different polynomial order α and dimensions L, d and w. We first analyzed four nanoantennas with $L = 50\,\mathrm{nm}$, $d = 10\,\mathrm{nm}$ and $\alpha = (1,2,3,4)$ for $N_t = 4608$, 5460, 6516, and 7896, with $\Delta v = 2.38 \times 2.38 \times 2.38\,\mathrm{nm}^3$, $\Delta v = 2 \times 2 \times 2\,\mathrm{nm}^3$, $\Delta v = 1.72 \times 1.72 \times 1.72\,\mathrm{nm}^3$ and $\Delta v = 1.5 \times 1.5 \times 1.5\,\mathrm{nm}^3$, respectively. The maximum fraction of the discretization to the wavelength is 2.38/500. With these discretizations we have a good convergence of the results. The thicknesses used in the simulations are $w = 9.5$; 10; 10.3; 10.6 (nm) for the antennas with $\alpha = (1,2,3,4)$ respectively. We also simulated nanoantennas with $\alpha = 3$ for different values of L and d. In these simulations, eight nanoantennas were analyzed with $L = 75$; 100; 125; 150 (nm) for fixed $d = 10\,\mathrm{nm}$, and $d = 5$; 15; 20; 25 (nm) for fixed $L = 50\,\mathrm{nm}$. The following sections present these results.

3.1. Near Field Distribution

In this section, we analyze the electric field distributions near the nanoantennas and its spatial confinement properties in the excitation regime. Firstly, we investigated the distributions of the electric field components x, y, and z for the antenna with $\alpha = 3$ at the main resonance $\lambda_a = 1030\,\mathrm{nm}$. The results are presented in Figure 3, where we observe that the values of the components x and z are larger than the component y in the plane $z = 10\,\mathrm{nm}$ (Figures 3(b)–(d)), and the x component (Figure 3(b)) is more confined in the antenna's gap. We

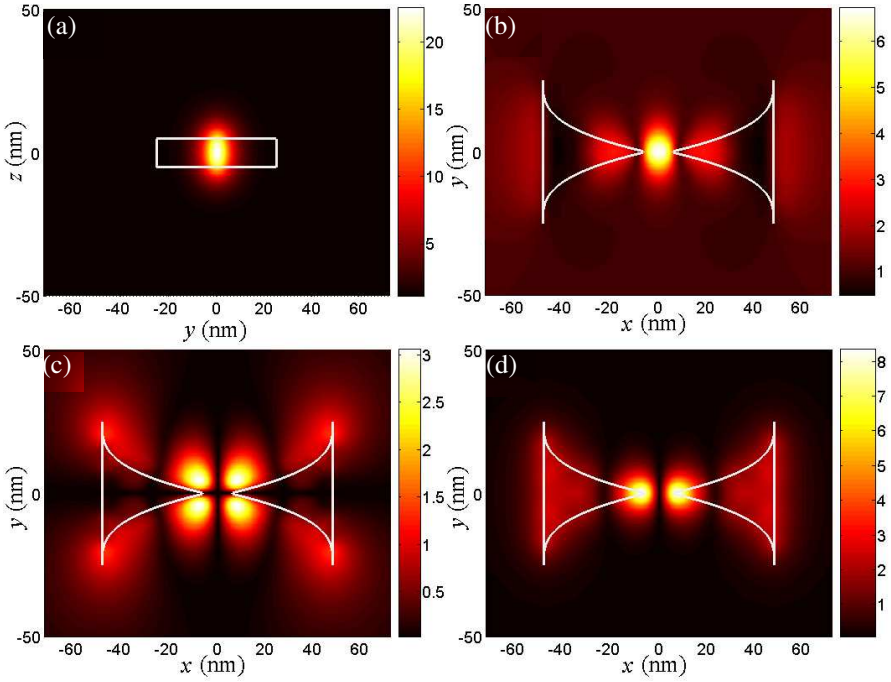

Figure 3. Near field distributions of the nanoantenna with $\alpha = 3$, $L = 50\,\text{nm}$, $d = 10\,\text{nm}$, $w = 10.3\,\text{nm}$ and $h = 43.3\,\text{nm}$ in $\lambda_a = 1030\,\text{nm}$. (a) $|E_x|/|E_0|$ in yz, and (b) $|E_x|/|E_0|$, (c) $|E_y|/|E_0|$, (d) $|E_z|/|E_0|$ in $z = 10\,\text{nm}$.

also observe that there is only the component x at the plane yz between the arms of the dipole (Figure 3(a)). From these results, we conclude that in the antenna's gap, the principal polarization is the component x. If a molecule is positioned in the middle of this dipole, the antenna's field will excite in the molecule a electric dipole moment $\bar{p}_e$ along the axis x, this is why we analyze in this paper only this polarization in the emission regime. The results of this emission regime will be presented in the next section.

To make a comparative analysis of field distributions of nanoantennas with different parameter α, Figure 4 shows the variation of the normalized total field near the nanoantennas with $\alpha = (1, 2, 3, 4)$ at the plane $z = 10\,\text{nm}$. This plane is approximately 5nm above the antenna's surface, because the antenna's thickness are variable, i.e., $w = 9.5$; 10; 10.3; 10.6 (nm) for the antennas with $\alpha = (1, 2, 3, 4)$ respectively. The dimensions of the antenna are $L = 50\,\text{nm}$ and $d =$

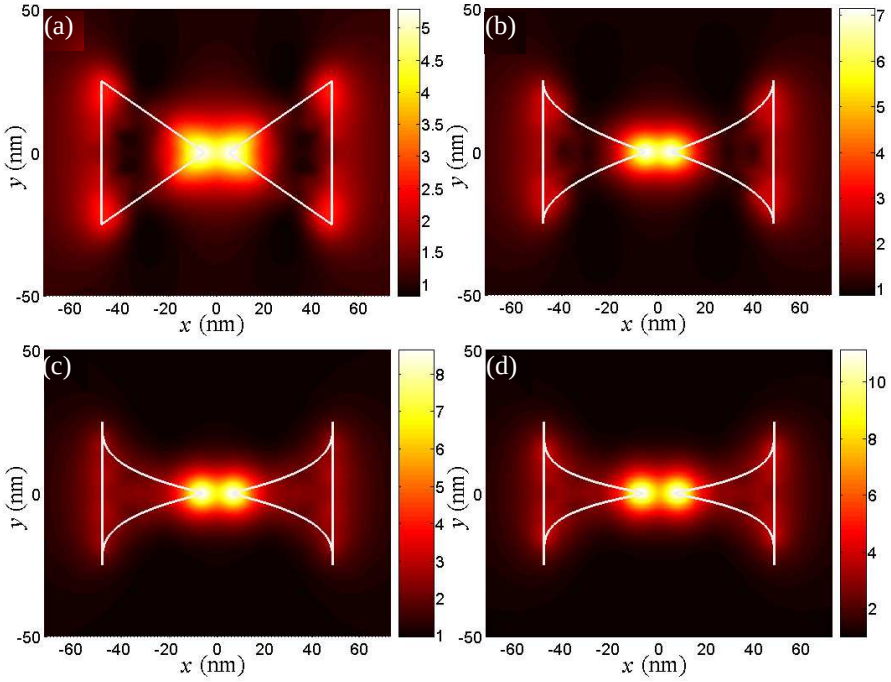

Figure 4. Normalized near field $|E|/|E_0|$ distribution at the plane $z = 10\,\text{nm}$ of the modified nanoantennas with $L = 50\,\text{nm}$, $d = 10\,\text{nm}$ and $h = 43.3\,\text{nm}$. (a) $\alpha = 1$ ($w = 9.5\,\text{nm}$) in $\lambda_a = 675\,\text{nm}$, (b) $\alpha = 2$ ($w = 10\,\text{nm}$) in $\lambda_a = 840\,\text{nm}$, (c) $\alpha = 3$ ($w = 10.3\,\text{nm}$) in $\lambda_a = 1030\,\text{nm}$, and (d) $\alpha = 4$ ($w = 10.6\,\text{nm}$) in $\lambda_a = 1194\,\text{nm}$.

10 nm, and the wavelength where these distributions were calculated are the principal resonances λ_a, that will be analyzed in the next section. In this figure, we observe the better field confinement of the modified antennas than that for the conventional one.

To analyze the spatial confinement, we present in Figure 5 the variation of the normalized field along the axis y and z. The spatial confinement parameters σ_y and σ_z are presented in Table 1. We note that these antennas possess higher confinement along the axis y than the axis z, and the highest confinement in the axis y is for the modified antennas with $\alpha = 2$, where $\sigma_y = 5.8\,\text{nm}$. The confinement in the axis y depends on the value of the polynomial order (α), and the confinement in the axis z depends on the antenna's thickness w. All the antennas in Figure 4 possess approximately the same values of w, this is why they have comparable values of σ_z.

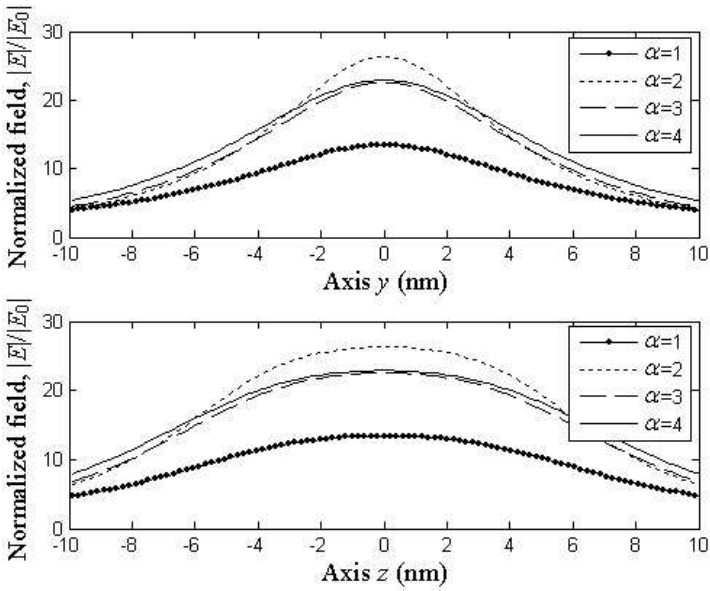

Figure 5. Field distributions along the axis y (upper) and z (down) of the modified nanoantennas with $L = 50\,\text{nm}$, $d = 10\,\text{nm}$ and $h = 43.3\,\text{nm}$, for $\alpha = 1$ ($w = 9.5\,\text{nm}$) in $\lambda_a = 675\,\text{nm}$, $\alpha = 2$ ($w = 10\,\text{nm}$) in $\lambda_a = 840\,\text{nm}$, $\alpha = 3$ ($w = 10.3\,\text{nm}$) in $\lambda_a = 1030\,\text{nm}$, and $\alpha = 4$ ($w = 10.6\,\text{nm}$) in $\lambda_a = 1194\,\text{nm}$.

3.2. Spectral Response in the Excitation Regime

Figure 6 shows the spectral response of the normalized field ($|E|/|E_0|$) in the middle of the antenna's gap (the origin of the coordinate system) and the scattering cross section in the $+z$ direction (SCS_z) of the nanoantennas with $\alpha = (1, 2, 3, 4)$. These characteristics were obtained by (3) and (4) in the excitation regime. We observe in these results two principal resonances in λ_a and λ_b ($\lambda_a > \lambda_b$), which are the same for the near field ($|E|/|E_0|$) and far field (SCS_z). The first resonance is the dipolar one and the second one represents the higher order multipolar resonances. These resonances are red shifted for large values of α, but the variation of λ_a is higher than λ_b. We conclude that the resonance λ_a is more sensitive with the geometric parameter α than the resonance λ_b, and this parameter can be used to tune the resonance of a particular antenna.

These results show that for a given bowtie nanoantenna with fixed values of L and d, the resonances can be controlled by the polynomial order α. This occurs because for larger values of α, the lengths of

the curved sides are higher, and the resonant wavelength λ_a of the dipole resonance is proportional to this length of the curved sizes. This resonant behavior is similar to the case of microwave antennas [27].

The values of $|E|/|E_0|$ and SCS_z at the resonances λ_a and λ_b are different. In the near field region, the main resonance is λ_a, where it presents highest values of $|E|/|E_0|$. In the far field region, the maximum values of SCS_z are obtained in λ_b, the exception is the case $\alpha = 2$ (Figure 6). Table 1 summarizes the values of some parameters of these antennas at the resonance λ_a. This table shows that the

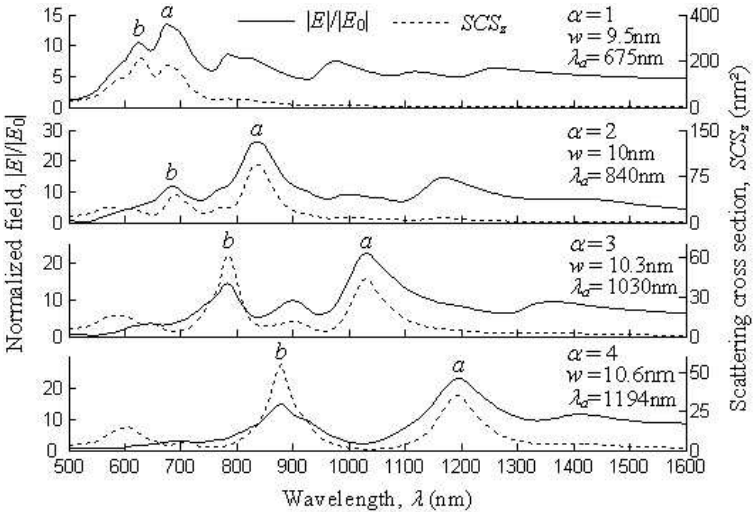

Figure 6. Spectral response of the normalized field in the middle of the antenna's gap and scattering cross section in the direction $+z$ of the modified bowtie nanoantennas with $\alpha = (1, 2, 3, 4)$ with $L = 50\,\text{nm}$, $d = 10\,\text{nm}$ and $h = 43.3\,\text{nm}$.

Table 1. Parameters of nanoantennas with $L = 50\,\text{nm}$, $d = 10\,\text{nm}$ and $h = 43.3\,\text{nm}$.

Parameter	$\alpha = 1$	$\alpha = 2$	$\alpha = 3$	$\alpha = 4$
Resonant wavelenght, λ_a (nm)	675	840	1030	1194
Field enhancement, $(\lvert E\rvert/\lvert E_0\rvert)^2$	180	692	508	524
Scattering cross section, SCS_z (nm^2)	180	93	44	35
Spatial confinement in y, σ_y (nm)	7.7	5.8	6.9	7.6
Spatial confinement in z, σ_z (nm)	11	10.4	11	11.8
Thickness, w (nm)	9.5	10	10.3	10.6

modified dipoles with $\alpha = (2, 3, 4)$ have higher field enhancement than the conventional one ($\alpha = 1$), and the highest value is 692 for the case $\alpha = 2$. The scattering cross section of antennas with larger values of α are smaller, this is due the different physical areas of the antennas.

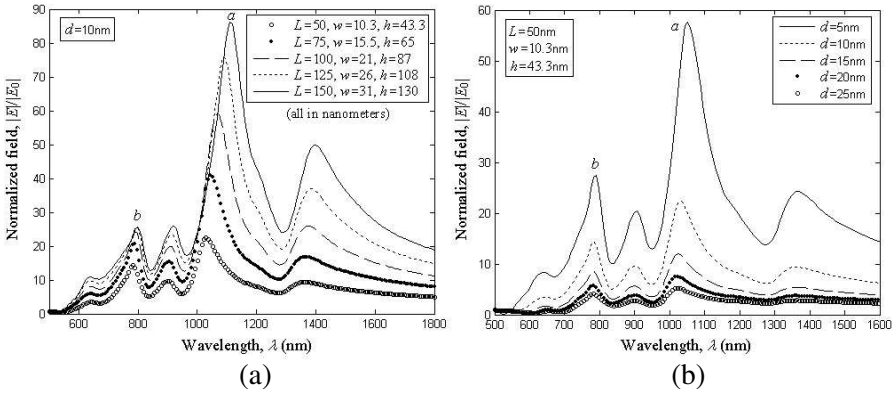

Figure 7. Variation of the spectral response of the normalized field in the middle of the antenna's gap for the nanoantenna with $\alpha = 3$. (a) Variation with the length L. (b) Variation with the length d.

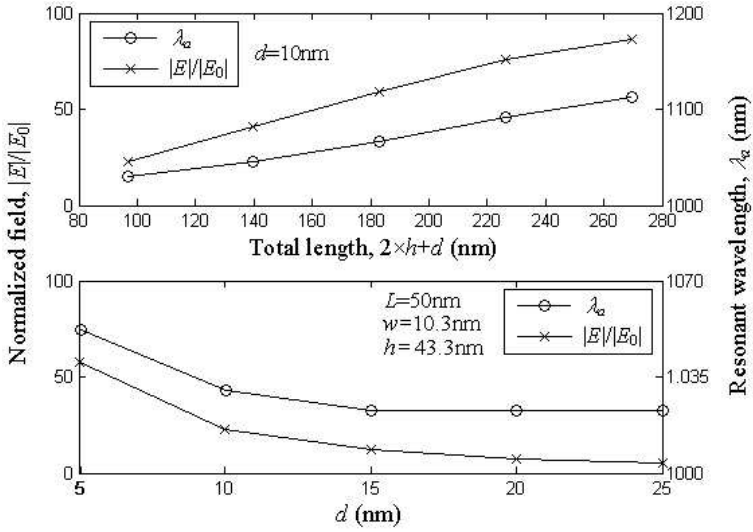

Figure 8. Variation of the normalized field and resonant wavelength λ_a versus the total antenna's length $2 \times h + d$ and versus distance between the arms of the nanoantenna d. These results are for the antenna with $\alpha = 3$.

Figure 7 presents the dependence of the spectral response of the antenna with $\alpha = 3$ on the lengths L and d. The parameter shown in these figures is the normalized field $|E|/|E_0|$ in the middle of the antenna's gap. Figure 8 shows the variation of the normalized field and resonant wavelength λ_a versus the total antenna's length $2 \times h + d$ and the distance between the arms of the dipole d. We observe in these figures that when the size L of the antenna is increased, the main resonance λ_a and the normalized field are almost linearly increased. On the other hand, the variation of these parameters with d are nearly constant for λ_a, and approximately exponential for $|E|/|E_0|$. For lower distances d, this normalized field increases rapidly.

3.3. Directivity and Efficiency in the Emission Regime

In this section, we present the numerical results of the modified bowtie nanoantennas in the emission regime, where an infinitesimal electric dipole localized in the middle of the nanoantennas is the source of the antenna system (Figure 1). The polarization of this infinitesimal dipole is in the x direction and its moment dipole is $\bar{p}_e$. This polarization was chosen because in the excitation mode only the component x of the electric field exists in the middle of the bowtie nanoantennas (Figure 3). The results presented here are the directivity D in the $+z$ direction ($\theta = 0^\circ$) and the radiation efficiency e as defined in (5) and (6) respectively.

Figure 9 presents the spectral response of D and e of the bowtie nanoantennas with $\alpha = (1, 2, 3, 4)$, for $L = 150\,\text{nm}$ and $d = 10\,\text{nm}$. We can see the maximum efficiency of each antenna occurs at the same resonant wavelengths λ_a and λ_b of the excitation regime. We also observe that the efficiencies of these resonances are reduced for larger values of α.

With respect the results of D in Figure 9, all the antennas possess $D \approx 1.5$ at the resonances λ_a and λ_b. This shows that these antennas have a radiation diagrams similar to that of an infinitesimal dipole in these resonances. The values of D near the wavelength $\lambda = 550\,\text{nm}$ are a little different of 1.5. We believe this is due the plasma resonance of Au, but this effect is not important in the analysis because it occurs far from the resonance of the antennas, where the radiation efficiency is very small. Thus, the radiation characteristics of these antennas are similar to those of electrically small antennas, because the total length $2 \times h + d$ of them are smaller than the resonant wavelengths λ_a and λ_b, so their directivities are constant in a wide range of the analyzed wavelengths.

To investigate the dependence of radiation efficiency e on the dimensions L and d, Figure 10 shows the variation of the spectral

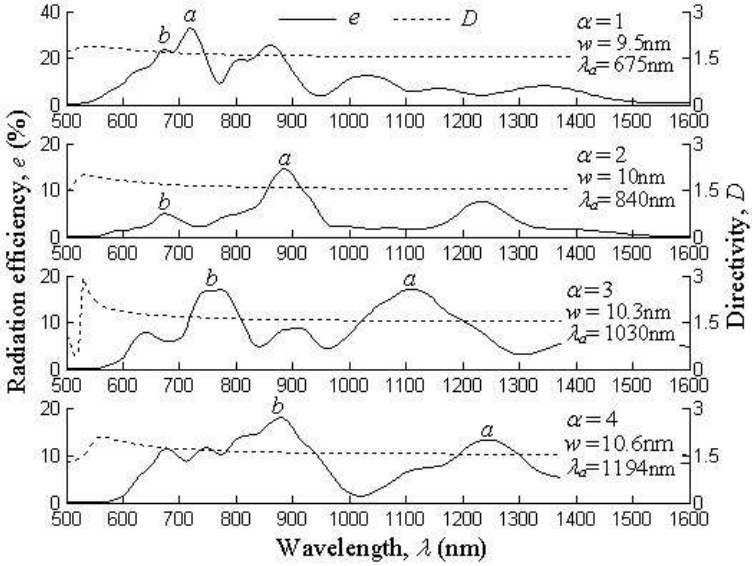

Figure 9. Radiation efficiency and directivity in $+z$ direction versus wavelength of the nanoantennas with $\alpha = (1, 2, 3, 4)$, for $L = 150\,\text{nm}$, $d = 10\,\text{nm}$ and $h = 43.3\,\text{nm}$.

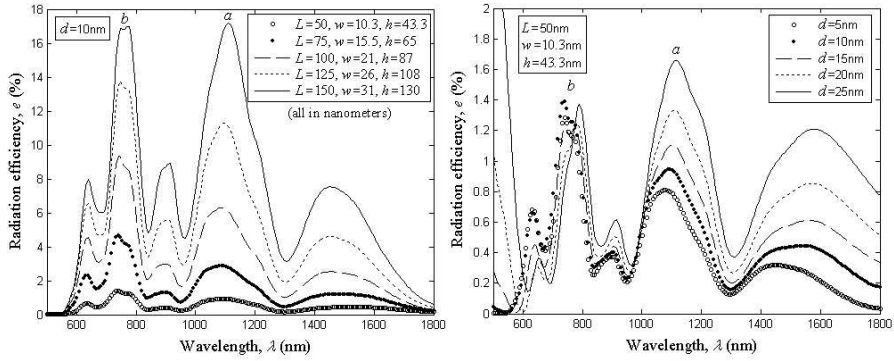

][

Figure 10. Variation of the spectral response of the radiation efficiency of the nanoantenna with $\alpha = 3$. (a) With the length L for $d = 10\,\text{nm}$. (b) With the distance d for $L = 50\,\text{nm}$.

response of e in function of the sizes L and d. These results were obtained for the nanoantenna with $\alpha = 3$, $d = 10\,\text{nm}$ in Figure 10(a) and $L = 50\,\text{nm}$ in Figure 10(b). We observe that the maximum efficiency also occur in the same resonant wavelengths λ_a and λ_b of the excitation regime presented in Figure 8. For larger values of L with d fixed, the antennas have better radiation efficiency, as well as for larger d with L fixed, they also have higher efficiency.

Figure 11 presents the variation of e at the resonances λ_a and λ_b in function of the total length $2 \times h + d$ and d. The results of these figures show that the radiation efficiency is very small for nanoantennas with $L = 50\,\text{nm}$, for example in $d = 10\,\text{nm}$ the efficiency is $e < 1\%$, but it increases exponentially with d. This approximately exponential variation is for the resonance of λ_a, and for the resonance of λ_b the efficiency remains practically constant. The increasing of e with $2 \times h + d$ is approximately linear for the two resonances λ_a and λ_b. These results are in accordance to those previously observed for conventional bowtie antennas with different values of L and d [9, 14].

With the results presented in this section, we conclude that the modified bowtie nanoantennas with $\alpha > 1$ possess smaller radiation

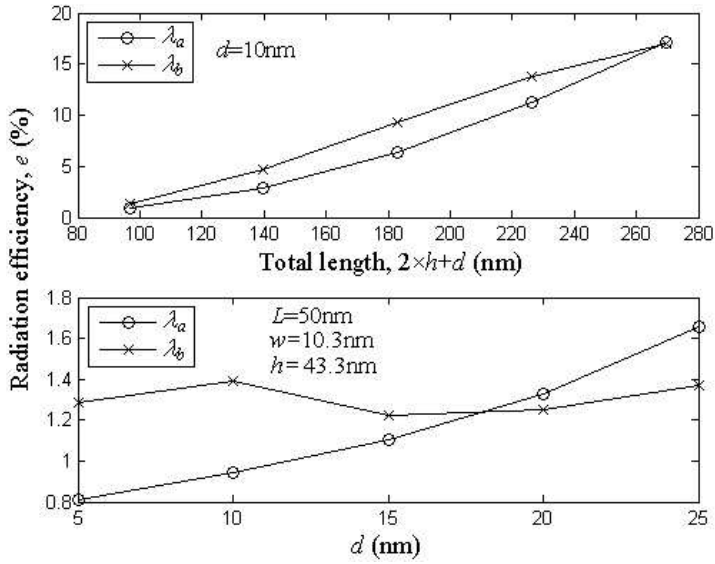

Figure 11. Variation of the radiation efficiency at resonances λ_a and λ_b versus (upper) the total antenna's length $2 \times h + d$ and (down) distance between the arms of the nanodipole d. These results are for the antenna with $\alpha = 3$.

efficiency than that of the conventional one with $\alpha = 1$ and their directivities are equal to 1.5 at the principal resonances. However, we can rise up the radiation efficiency with the increasing of the dimensions L and d.

4. CONCLUSIONS

In this paper, we presented a theoretical analysis of modified bowtie nanoantennas with polynomial sides in the excitation and emission regimes. We observed in the excitation regime that the resonances of the modified antennas are shifted to higher wavelengths and the electric field in the middle of the gap's antenna is increased, where it presents only polarization along the axis of the dipoles. Also, the field confinements of the modified antennas are higher than the conventional one. In the emission mode, we noted that the maximum radiation efficiency of all antennas occurs at the same resonant wavelengths obtained in the excitation regime, and the values of these efficiencies, for the modified antennas, are smaller than those of the conventional one with the same dimensions, but it can be increased for larger antenna's size and gap distances between the arms of the dipoles. With respect the directive properties of these antennas, all the cases analyzed presented directivities similar to that of an electrically small antenna.

With all these results, we conclude that the modified bowtie nanoantennas have higher near field enhancement and confinement, and smaller radiation efficiency than those of the conventional bowtie antenna with linear sides. With appropriately chosen dimensions, these novel nanoantennas can be used, for example, to enhance the spontaneous emission of single molecules positioned in the middle of the antenna's gap. Future works can be the analysis the characteristics dependence of these antennas on the thickness, orientation of the incident plane wave, and the polarization of the emitter in the gap.

ACKNOWLEDGMENT

This work was financially supported by the Brazilian agency CNPq.

REFERENCES

1. Novotny, L., *Principles of Nano-optics*, Cambridge, New York, 2006.
2. Wang, H., C. T. Chong, and L. Shi, "Optical antennas and their potential applications to 10 terabit/in recording," *Opt. Data Storage Top. Meet.*, 16–18, 2009.

3. Sqalli, O., I. Utke, P. Hoffmann, and F. M. Weible, "Gold elliptical nanoantennas as probes for near field optical microscopy," *J. of Appl. Physics*, Vol. 92, 1078–1083, 2002.
4. Lyshevski, S. E. and M. A. Lyshevski, "Nano- and microopto-electromechanical systems and nanoscale active optics," *Third IEEE Conf. on Nanotechnology*, 2003.
5. Huang, J. S., T. Feichtner, P. Biagioni, and B. Hecht, "Impedance matching and emission properties of nanoantennas in an optical nanocircuit," *Nano Lett.*, Vol. 9, 1897–1902, 2009.
6. Fromm, D. P., A. Sundaramurthy, A. Kinkhabwala, P. J. Schck, G. S. Kino, and W. E. Moerner, "Exploring the chemical enhancement for surface-enhanced Raman scattering with Au bowtie nanoantennas," *The J. of Chem. Phi.*, Vol. 124, 2006.
7. Parajo, M. F. G., "Optical antennas focus in on biology," *Nat. Phot.*, Vol. 2, 201–203, 2008.
8. Mhlschlegel, P., et al., "Resonant optical antennas," *Science*, Vol. 308, 1607–1609, 2005.
9. Fischer, H. and O. J. F. Martin, "Engineering the optical response of plasmonic nanoantennas," *Opt. Express*, Vol. 16, 9144–9154, 2008.
10. Liaw, J. W., "The quantum yield of a metallic nanoantenna," *Appl. Phys. A*, Vol. 89, No. 10, 357–362, 2007.
11. Giannini, V., J. A. Sánchez-Gil, O. L. Muskens, and J. G. Rivas, "Electrodynamic calculations of spontaneous emission coupled to metal nanostructures of arbitrary shape: Nanoantenna-enhanced fluorescence," *J. Opt. Soc. Am. B*, Vol. 26, 1569–1577, 2009.
12. Kern, A. M. and O. J. F. Martin, "Excitation and reemission of molecules near realistic plasmonic nanoestructures," *Nano Lett.*, Vol. 11, 482–487, 2011.
13. Taminiau, T. H., F. D. Stefani, and N. F. V. Hulst, "Enhanced directional excitation and emission of single emitters by a nano-optical Yagi-Uda antenna," *Opt. Express*, Vol. 16, 16858–16866, 2008.
14. Wu, Y. M., L. W. Li, and B. Liu, "Geometric effects in designing bow-tie nanoantenna for optical resonance investigation," *Asia-Pacific Int. Symp. on Electromagnetic Compatibiliy*, 1108–1111, 2010.
15. McMahon, J. M., S. K. Gray, and G. C. Schatz, "Optical properties of nanowires dimers with a spatially nonlocal dielectric function," *Nano Lett.*, Vol. 10, 3473–3481, 2010.
16. Liaw, J. W., "Analysis of a bowtie nanoantenna for the

enhancement of spontaneous emission," *IEEE J. Selec. Top. Qua. Elec.*, Vol. 14, 1441–1447, 2008.

17. Kinkhabwala, A., et al., "Large single-molecule fluorescence enhancements produced by a bowtie nanoantenna," *Nat. Photonics*, Vol. 3, 654–657, 2009.
18. Livesay, D. E. and K. M. Chen, "Electromagnetic fields induced inside arbitrary shaped biological bodies," *IEEE Trans. Micro. Theo. Thec.*, Vol. 22, 1273–1280, 1974.
19. Girard, C., E. Dujardin, G. Baffou, and R. Quidant, "Shaping and manipulation of light fields with bottom-up plasmonic structures," *New J. of Physics*, Vol. 10, 105016, 2008.
20. Gu, Y., J. Li, Q. J. F. Martin, and Q. Gong, "Solving surface plasmon resonances and near field in metallic nanostructures: Green's matrix method and its applications," *Chinese Science Bulletin*, Vol. 55, 2608–2617, 2010.
21. Ewe, W. B., H. S. Chu, E. P. Li, and E. W. Li, "Investigation of surface plasmon resonance of nanoparticles using volume integral equation," *Proc. Asia-Pacific Microwave Conference*, 2007.
22. Giannini, V. and J. A. S. Gil, "Calculations of light scattering from isolated and interacting metallic nanowires of arbitrary cross section by means of Green's theorem surface integral equations in parametric form," *J. Opt. Soc. Am. A*, Vol. 24, 2822–2830, 2007.
23. Yang, Z. Y., et al., "FDTD for plasmonics: Applications in enhanced Raman spectroscopy," *Chinese Science Bulletin*, Vol. 55, 2635–2642, 2010.
24. Draine, B. D. and P. J. Flatau, "Discrete-dipole approximation for scattering calculations," *J. Opt. Soc. Am. A*, Vol. 11, 1491–1499, 1994.
25. Wu, Y. M., L. W. Li, and B. Liu, "Gold bow-tie shaped aperture nanoantenna: Wide band near-field resonance and far-field radiation," *IEEE Trans. on Magnetics*, Vol. 46, 1918–1921, 2010.
26. Costa, K. Q. and V. Dmitriev, "Comparative analysis of circular and triangular gold nanodisks for field enhancement applications," *J. of Microwaves, Optoelectronics and Electromagnetic Applications*, Vol. 9, 123–130, 2010.
27. Balanis, C. A., *Antenna Theory: Analysis and Design*, John Wiley & Sons, Inc., New Jersey, 2005.